Nanoscale

ROYAL SOCIETY OF CHEMISTRY

COMMUNICATION

View Article Online
View Journal | View Issue

Cite this: *Nanoscale*, 2022, **14**, 305

Received 20th September 2021,
Accepted 30th November 2021

DOI: 10.1039/d1nr06200j

rsc.li/nanoscale

Red-emissive nanocrystals of $Cs_4Mn_xCd_{1-x}Sb_2Cl_{12}$ layered perovskites†

Emanuela Sartori, [a,b] Marta Campolucci,[a,b] Dmitry Baranov, [b] Min Zeng, [c,d] Stefano Toso, [b,e] Giorgio Divitini, [f] Maurizio Ferretti,[a] Zeger Hens, [d] Liberato Manna [b] and Federico Locardi *[a,b,d]

Layered double perovskites are currently being investigated as emerging halide-based materials for optoelectronic applications. Herein, we present the synthesis of $Cs_4Mn_xCd_{1-x}Sb_2Cl_{12}$ ($0 \leq x \leq 1$) nanocrystals (NCs). X-ray powder diffraction evidences the retention of the same crystal structure for all the inspected compositions; transmission electron microscopy revealed monodisperse particles with a mean size between 10.7 nm and 12.7 nm. The absorption spectra are mostly determined by transitions related to Sb^{3+}, whereas Mn^{2+} induced a red emission in the 625–650 nm range. The photoluminescence emission intensity and position vary with the Mn^{2+} content and reach the maximum for the composition with $x = 0.12$. Finally, we demonstrate that the photoluminescence quantum yield of the latter NCs was increased from 0.3% to 3.9% through a post-synthesis treatment with ammonium thiocyanate. The present work expands the knowledge of colloidal layered double perovskite nanocrystals, stimulating future investigations of this emerging class of materials.

[a]*Department of Chemistry and Industrial Chemistry, Università degli Studi di Genova, Via Dodecaneso 31, 16146 Genova, Italy. E-mail: federico.locardi@unige.it*
[b]*Nanochemistry Department, Istituto Italiano di Tecnologia, Via Morego 30, 16163, Italy*
[c]*Hubei Key Laboratory of Ferro- & Piezoelectric Materials and Devices, Faculty of Physics and Electronic Science, Hubei University, Wuhan, 430062, P. R. China*
[d]*Physics and Chemistry of Nanostructures group (PCN), Ghent University, Krijgslaan 281, Gent 9000, Belgium*
[e]*International Doctoral Program in Science, Università Cattolica del Sacro Cuore, 25121 Brescia, Italy*
[f]*Electron Spectroscopy and Nanoscopy, Istituto Italiano di Tecnologia, Via Morego 30, 16163, Italy*
†Electronic supplementary information (ESI) available. See DOI: 10.1039/d1nr06200j

Federico Locardi

Dr Federico Locardi received his PhD in Chemical Science from the University of Genoa (Italy), in 2015. He completed his first postdoctoral studies at the University of Genoa and Nanochemistry Department of IIT (Istituto Italiano di Tecnologia), focusing on the synthesis of halide perovskite nanocrystals. In 2019, he moved to the Physics and Chemistry of Nanostructures group at Ghent University (Belgium); after one year, he returned to the University of Genoa, where he is an assistant professor at the Department of Chemistry and Industrial Chemistry. His research focuses on the development of new inorganic (nano)materials for photocatalysis and optoelectronics.

Introduction

In recent years, extensive research on lead halide perovkistes[1] has led to increasing interest in new metal halides with a wide variety of structures and compositions based on different transition metals.[2] In particular, the concerns about the toxicity and limited stability of lead-based compositions have inspired researchers to explore alternatives, with comparable or, ideally, even better optoelectronic properties.[3,4] Double perovskites (DPs) represent one of the first attempts towards lead substitution. In DPs, the original 3D structure of lead halides, *i.e.* a framework composed of corner-sharing $[PbX_6]$ ($X = Cl^-$, Br^-, I^-) octahedra, is retained by the alternation of octahedra formed by monovalent and trivalent cations.[5] In this way, charge neutrality is maintained, as expressed through the general chemical formula $A_2M^+M^{3+}X_6$ (M = metal, $X = Cl^-$, Br^-, I^-). Several combinations of M^+ and M^{3+} cations have been tested, both in bulk and in nanocrystals (NCs), for example $M^+ = Ag^+$, Na^+, K^+ and $M^{3+} = In^{3+}$, Bi^{3+}, Sb^{3+}.[6–12] In this kind of structure, the need to maintain the charge balance and the constraints imposed by the ionic radii make the introduction of bivalent metal cations (M^{2+}) generally possible only at low concentrations.[12–14]

Complete substitution of the M^+ cations with M^{2+} cations is possible with the concomitant introduction of a vacancy (Vac),

resulting in a general $A_4M^{2+}M^{3+}{}_2X_{12}$ stoichiometry; these materials, due to their peculiar structure, are commonly known as ⟨111⟩ oriented layered double perovskites (LDPs).[2] Indeed, the structure can be described as a cubic substructure of Cs^+ cations[15] filled alternatively by layers of corner-sharing $[M^{2+}X_6]$–$[M^{3+}X_6]$–$[M^{2+}X_6]$–$[VacX_6]$ octahedra along the ⟨111⟩ direction. The first LDP, $Cs_4CuSb_2Cl_{12}$, was synthesized as a bulk material by Solis-Ibarra's group in 2017 and had an optical bandgap of 1 eV, which is promising for photovoltaics;[16] Cai *et al.* prepared the same composition as NCs, with optical properties in line with those of the corresponding powders.[17] The partial substitution of Cu^{2+} with Mn^{2+} tunes the band gap to higher energy, and a low-intensity red emission was measured from $Cs_4MnSb_2Cl_{12}$.[18] A more efficient emission has been observed with the partial introduction of Cd^{2+},[19] leading to a photoluminescence quantum yield (PLQY) of 37.5% for $Cs_4Cd_{0.75}Mn_{0.25}Sb_2Cl_{12}$.[20] The replacement of Sb^{3+} with Bi^{3+} resulted in an increase of the PLQY[21] up to 79.5% for the $Cs_4Cd_{1-x}Mn_xBi_2Cl_{12}$ (x = 0.1) composition.[22] Yang *et al.* successfully synthesized the same series in the form of nanocrystals; however, the resulting materials exhibited a 20-fold drop of the PLQY (4.6%) compared to bulk crystals.[23]

LDPs have been proposed as optoelectronic materials for LEDs[2,19] and high-speed photodetection[20,24] due to the strong anisotropy in their crystal structure. Moreover, preliminary studies have been conducted to investigate their magnetic behavior for potential applications in ferroelectrics and spintronics.[2,25]

Motivated by the aforementioned studies and by the need to expand the range of the available stoichiometries of LDPs at the nanoscale, we devised a synthesis of $Cs_4Cd_{1-x}Mn_xSb_2Cl_{12}$ in the form of NCs. Using a hot injection approach, we found that alloying Cd^{2+} and Mn^{2+} is possible (that is, x in the above formula can range from 0 to 1) with the formation of phase-pure cuboidal nanoparticles. The optical characterization has revealed a red emission centered at 625–650 nm for all the samples, except for x = 0, with the emission position and intensity depending on the Mn^{2+} content. The sample with x = 0.12 yielded the most intense emission of the series, with a PLQY of 0.3% that was further enhanced ten-fold to 3.9% by means of surface treatment with ammonium thiocyanate. Overall, our work expands the knowledge of the layered double perovskite at the nanoscale, highlighting the potential of these compounds as optoelectronic materials.

Results and discussion

We prepared $Cs_4Mn_xCd_{1-x}Sb_2Cl_{12}$ NCs by a hot-injection method. Briefly, the synthesis consisted of degassing the precursors (metal acetates and carbonates) under vacuum in a mixture of dioctyl ether, oleylamine, and oleic acid for 20 minutes at 115 °C, followed by an injection of benzoyl chloride at 160 °C under a N_2 atmosphere (Scheme 1; see the ESI† for details). The resulting nanoparticles had a cuboidal

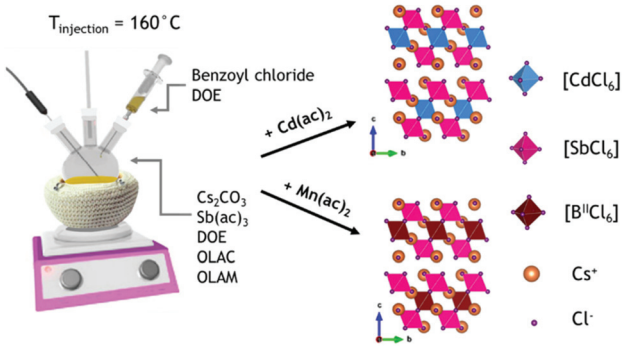

Scheme 1 Colloidal synthesis of $Cs_2Mn_xCd_{1-x}Sb_2Cl_{12}$ ($0 \le x \le 1$) NCs.

shape for all the inspected samples, with a Mn^{2+} content tunable by systematically changing the $Mn^{2+}/(Cd^{2+} + Mn^{2+})$ precursor ratio from 0 to 1. The ICP-OES analysis revealed that, in general, an amount of Mn^{2+} lower than the one loaded actually enters the structure, especially when the $Mn^{2+}/(Cd^{2+} + Mn^{2+})$ ratio of the precursors is lower than 0.5 (Table S1 and Fig. S1†); a similar phenomenon was observed in $Cs_4Mn_xCd_{1-x}Bi_2Cl_{12}$.[21]

The powder X-ray diffraction (XRD) data indicated that all the synthesized compositions crystallize always in the trigonal $R\bar{3}m$ structure (Fig. 1a and S2†) and the samples with intermediate x were phase-pure and isostructural to the terminal compositions (x = 0 and 1, Fig. 1b and S2†). The shape of nanocrystals reflected the influence of the cuboidal Cs^+ substructure, as commonly observed for other metal–halide perovskite nanocrystals.[15] The slight shift of the diffraction peaks toward higher 2θ angles (Fig. 1b right) originates from the contraction of the unit cell due to the substitution of the Cd^{2+} cations with the smaller Mn^{2+} cations. Indeed, the cell parameters shifted from a = 7.586 Å, c = 37.165 Å to a = 7.549 Å, c = 36.994 Å for 0% Mn^{2+} and 100% Mn^{2+}, respectively. The unit cell contracted by 1.44% in volume, and the contraction was found to be isotropic (a = −0.49%; c = −0.46%), suggesting a random Mn^{2+}/Cd^{2+} replacement in the structure (Fig. S3†). These results agree with the data reported on the corresponding powders.[19] Transmission electron microscopy (TEM) micrographs of $Cs_4Mn_xCd_{1-x}Sb_2Cl_{12}$ NCs evidenced the formation of NCs with a cuboidal shape (Fig. 1c–f), and a mean size of 10.7 ± 3.5 nm and 12.4 ± 3.8 nm for 0% and 100% Mn^{2+}, respectively; for the larger Mn^{2+} fractions (x = 0.9, 1) smoothing of the NC edges occurred (Fig. 1f and S4†). High-angle annular dark-field (HAADF) scanning TEM imaging confirmed the crystallinity of the NCs (Fig. 1g and S5†), most often composed of a single crystal domain; occasionally, multiple domains were observed in particles larger than 20 nm (Fig. S5†). Elemental analysis confirmed that all the expected elements are included in the NCs (Fig. S6†). Upon changing the injection temperature (*i.e.* 140–150–170 °C), we observed no changes in the crystal structure (Fig. S7a†), yet higher temperatures led to NC samples with a more polydisperse distribution of size and morphology (Fig. S7b–e†).

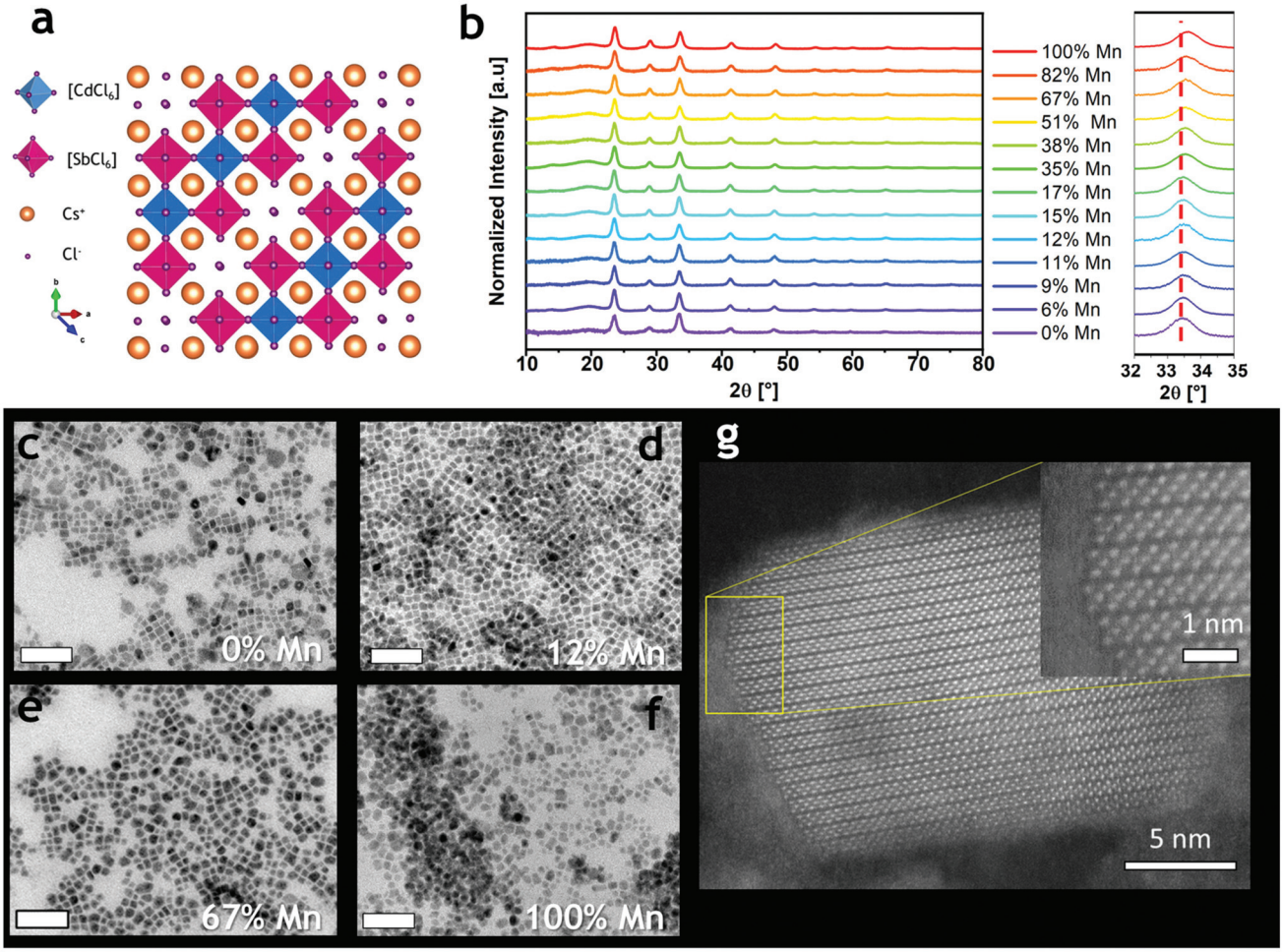

Fig. 1 (a) Crystal structure of $Cs_4CdSb_2Cl_{12}$; (b) XRD patterns of $Cs_4Mn_xCd_{1-x}Sb_2Cl_{12}$ NCs; a shift to higher angles on increasing the Mn^{2+} amount was observed (right); (c–f) bright-field TEM micrographs of $Cs_4Mn_xCd_{1-x}Sb_2Cl_{12}$ NCs. Scale bars are 100 nm; (g) HAADF-STEM image of a single nanocrystal of the $Cs_4Mn_{0.12}Cd_{0.88}Sb_2Cl_{12}$ sample.

All samples displayed an absorption spectrum characterized by three different features: two broad peaks between 300 nm and 400 nm (Fig. 2a and S8a†) that were independent of the $Mn^{2+}/(Cd^{2+} + Mn^{2+})$ ratio, and a well-defined peak at 267 nm (for $x = 0$) whose intensity decreased with a concomitant blue shift with the increasing Mn^{2+} amount (Fig. S8a†). The observed behavior is consistent with the corresponding bulk material except for the intensity variation and shift of the last spectral feature (250–300 nm), which was previously not observed by Solis-Ibarra's group.[19] Overall, the absorption spectrum of $Cs_4Mn_xCd_{1-x}Sb_2Cl_{12}$ seems to be mostly determined by transitions related to Sb^{3+}, not unlike previous observations on $Cs_3Sb_2Cl_9$.[26] Sb^{3+} is an ns^2 ion characterized by the $^1S_0$ ground state and four higher-energy levels denoted as $^3P_0$, $^3P_1$, $^3P_2$ and $^1P_1$.[27] The absorption in the 300–400 nm range can be ascribed to the partially allowed $^1S_0 \rightarrow {}^3P_1$ transition, commonly named the A band, split into a doublet; similarly, the allowed $^1S_0 \rightarrow {}^1P_1$ transition (C band) is responsible for the absorption found at ~270 nm.[11,19,27,28] Instead, the d → d Mn^{2+} transition, generally observed for Mn-based materials between 400 nm and 550 nm, was not detected. All the $Cs_4Mn_xCd_{1-x}Sb_2Cl_{12}$ compositions, except for $x = 0$, showed a red emission centered at around 625–650 nm under UV excitation (Fig. S8b†). The photoluminescence excitation (PLE) spectra exhibited an intense peak centered at ~325 nm with a shoulder at ~285 nm (Fig. 2b). The PLE behavior resembled that of absorption, indicating that the excitation occurs through the Sb^{3+} bands. Interestingly, even if Sb^{3+} is known for exhibiting optical emission in metal halides,[27,29] we did not detect any PL signals in $Cs_4CdSb_2Cl_{12}$, whereas the $^4T_1 \rightarrow {}^6A_1$ transition of Mn^{2+} induced the red emission in all the other samples. We explain this behavior by an energy transfer between antimony(III) and manganese(II) ions, $Sb^{3+} \rightarrow Mn^{2+}$.[30] Indeed, the PLE profiles were the same for all the samples, with no considerable shift (Fig. S8c†), while significant differences were detected both in the PL intensity and positions (Fig. 2c, d and S8b†). No differences in the PL were observed when exciting the samples at a different wavelength (Fig. 2b). The intensity increased with the Mn^{2+} ratio (Fig. 2c) up to a maximum at the experimental composition of 11.5% Mn^{2+}.

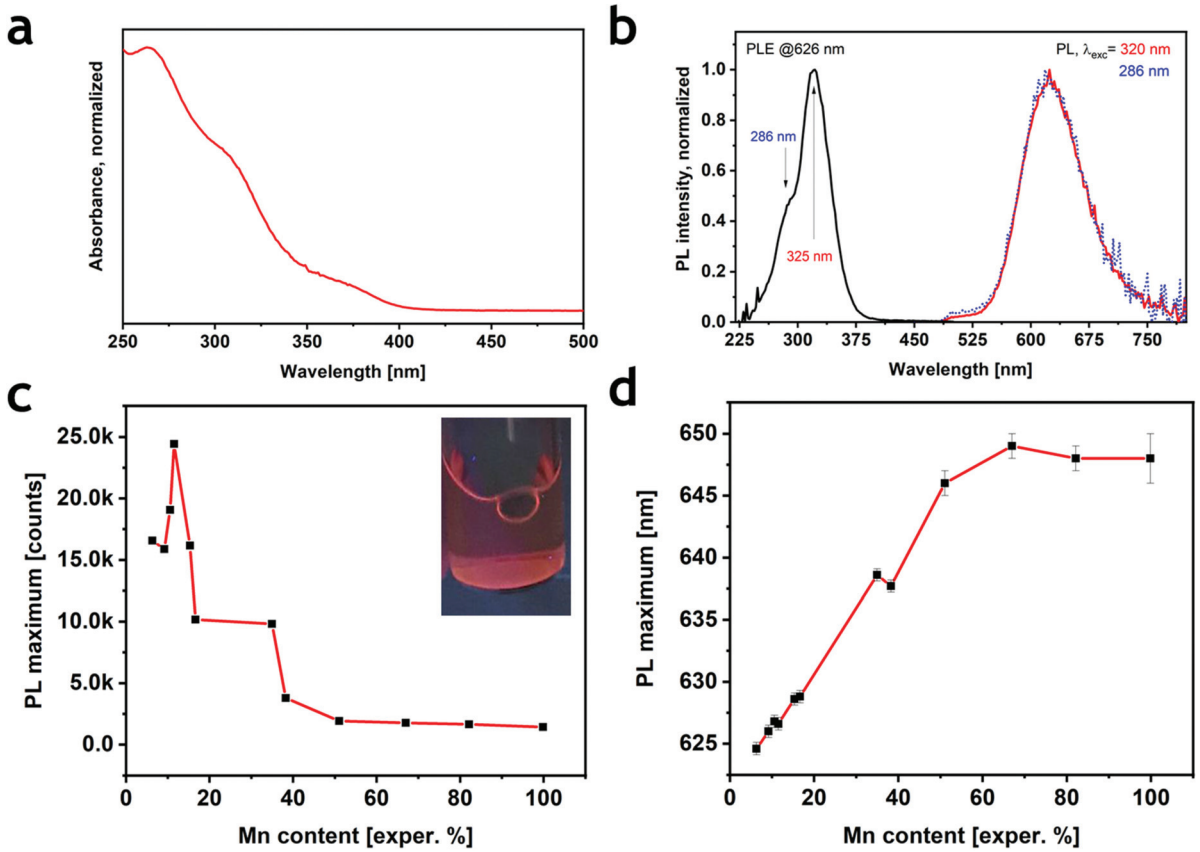

Fig. 2 (a) Optical absorption at 250 nm and (b) PLE and PL spectra measured at two different excitation wavelengths (320 nm and 286 nm) of the $Cs_4Mn_{0.12}Cd_{0.88}Sb_2Cl_{12}$ sample chosen as a representative. (c) PL intensity (normalized at the absorption at 320 nm) behavior at increasing Mn^{2+} content; the inset shows a photograph of the most emissive sample under UV light. (d) Position of the PL peak with increasing Mn^{2+} content.

Similar results were reported for the corresponding bulk system.[19] By increasing the Mn^{2+} concentration the emission gradually shifted from 624 nm (6% Mn^{2+}), a value higher than that in bulk $Cs_4Mn_xCd_{1-x}Sb_2Cl_{12}$ [19,20] but close to reports for the Bi-based counterpart $Cs_2MnBi_2Cl_{12}$,[21,23] to a roughly constant spectral position of ~648 nm for $x > 0.5$ (Fig. 2d). The Mn^{2+} emission shift was already reported in $Cs_4Mn(Bi_{1-x}In_x)_2Cl_{12}$ [31] and $CsPbCl_3$,[32,33] and ascribed to a contraction of the unit cell; according to the Tanabe–Sugano diagram for the d^5 ion (*e.g.* Mn^{2+}), an increase of the crystal field induces a red shift in the $^4T_1 \rightarrow {}^6A_1$ transition. Indeed, the progressive substitution of Cd^{2+} with the smaller Mn^{2+} decreased the cell volume by shrinking the $[MnCl_6]$ octahedra,[19] thus inducing the observed red shift. The variation of the PL intensity can be instead explained considering that the maximum intensity is reached, in principle, when the $MnCl_6$ octahedra are surrounded by $[SbCl_6]$ and $[CdCl_6]$ octahedra, thus, avoiding any Mn–Mn self-quenching.[23]

The PLQY of the most emissive colloidal sample was found to be 0.3%, a value that is much lower than that reported for the corresponding bulk material (28.5%).[19] The decrease of PLQY with reduced particle size has been previously observed in $Cs_4Mn_xCd_{1-x}Bi_2Cl_{12}$: when lowering the dimensions of the particles from micrometers to nanometers, the PLQY collapsed from 79.5%[22] to 4.6%.[23] This unfavorable effect, already documented in several metal–halide perovskites, can be ascribed to the formation of non-radiative relaxation paths induced by surface traps. To test this hypothesis, we attempted three different post-synthetic treatments to increase the PLQY of the nanocrystals: a small fraction of the nanocrystal suspension was added to (i) a mixture of $CdCl_2$, OA and OlAm in hexane;[32,34] (ii) a solution of didodecyldimethylammonium chloride (DDAC) in toluene;[35] and (iii) a mixture of ammonium thiocyanate (NH_4SCN) in hexane[36,37] (see the ESI and Table S2†). The first two treatments slightly increased the photoluminescence, while a significant enhancement was observed when using NH_4SCN (Fig. S9†); consequently, only the sample treated with NH_4SCN was investigated. During the treatment, the sample emission kept increasing for one hour (Fig. S9†), after which it started decreasing due to the progressive decomposition of the sample, which completely evolved in other phases after three hours (Fig. S10†). The XRD and TEM analyses on the brightest sample (Fig. 3a) showed that the crystalline phase was preserved, even if a small amount of a secondary phase, identified as CsCl, was present. As determined by TEM, the morphology of the NCs was largely preserved, but cuboidal shapes appeared more rounded compared to the pristine sample (Fig. 3b and c). The absorption spectrum revealed

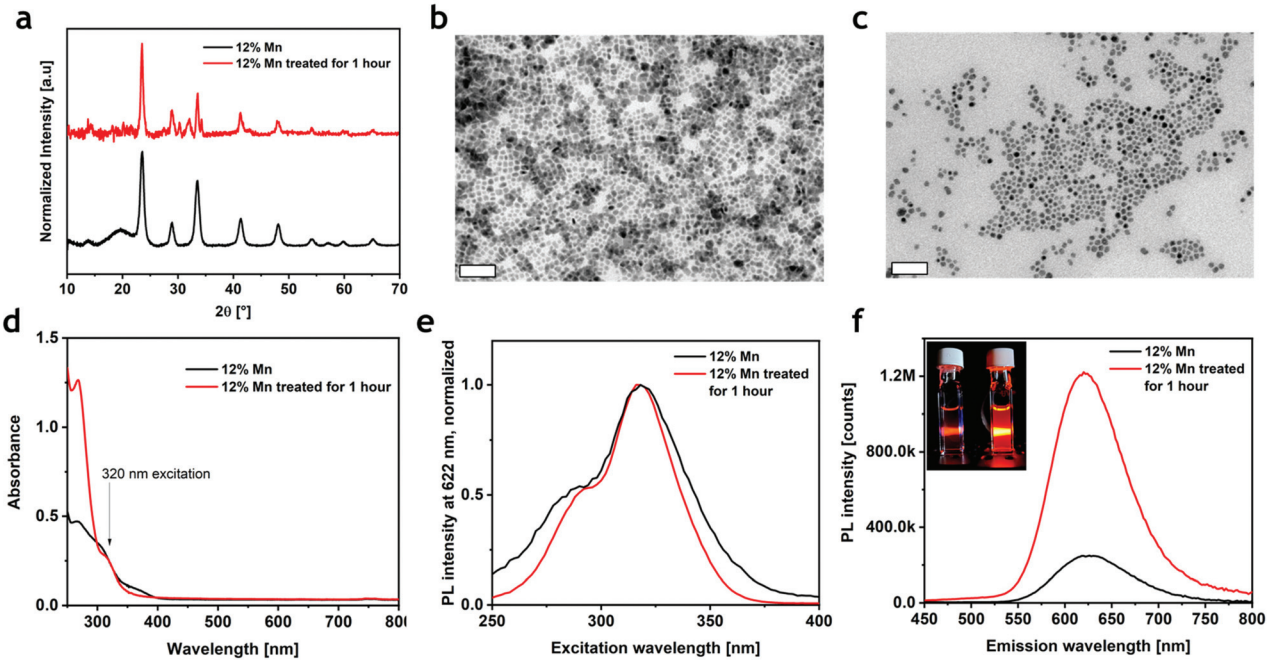

Fig. 3 (a) XRD pattern of $Cs_4Mn_{0.12}Cd_{0.88}Sb_2Cl_{12}$ before (black line) and after the thiocyanate treatment (red line). (b) and (c) bright-field TEM images before and after the thiocyanate treatment, respectively. (d) ABS, (e) PLE, and (f) PL of $Cs_4Mn_{0.12}Cd_{0.88}Sb_2Cl_{12}$ before (black line) and after thiocyanate treatment (red line). Inset in (f) shows a photograph under a UV lamp of the sample with (bright orange) and without the treatment (dark orange).

a small decrease in the 350–400 nm range and an enhancement of the C band (λ < 300 nm) (Fig. 3d). Furthermore, the PLE spectrum narrowed without a significant shift (Fig. 3e). More importantly, an enhanced PL emission was observed, which resembled the same broadness of the pristine material with a small shift of ~2 nm (Fig. 3f and S11†). The conservation of the PLE and PL spectral shapes and positions suggests that the post-treatment does not influence the environment around Mn^{2+} (*i.e.*, the crystal structure); as previously demonstrated in other halide perovskites,[36,38,39] the thiocyanate group passivates the surface sites removing the shallow trap and reducing the number of non-radiative relaxation channels. Indeed, the PLQY of the material after the post-synthesis treatment reached a value of 3.9% (Fig. S12†), which is 10 times higher than that in the as-synthesized particles, and comparable to that of the Bi-based counterpart.

Conclusions

In summary, we successfully synthesized $Cs_4Mn_xCd_{1-x}Sb_2Cl_{12}$ nanocrystals with tunable composition in the x = 0–1 range. All the samples showed a UV absorption and a red emission stemming from Sb^{3+} and Mn^{2+} ions (except for the Mn-free x = 0), respectively. The PL intensity changed with the Mn^{2+} amount, reaching a maximum for x = 0.12. The pristine sample featured a low PLQY (<1%) that was increased to 3.9% by a post-synthesis treatment with ammonium thiocyanate. The intriguing optical properties of $Cs_4Mn_xCd_{1-x}Sb_2Cl_{12}$ nanocrystals should stimulate additional studies on this emerging family of layered double perovskites and their application as optoelectronic materials.

Author contributions

E.S. – conceptualization, data curation, formal analysis, investigation (synthesis, XRD, TEM, ICP-OES, and optical analysis), validation, visualization (figures) and writing (original draft); M.C. – data curation, formal analysis, investigation (synthesis, XRD, TEM, and optical analysis), and validation; D.B. – data curation, formal analysis, investigation (optical analysis), and writing (editing); M.Z. – data curation, formal analysis, and investigation (XRD, optical analysis); S.T. – formal analysis and investigation (XRD); G.D. – investigation (HAADF – STEM); M. F. – conceptualization, supervision, and writing (review and editing); Z.H. – conceptualization, supervision, and writing (review and editing); L.M. – conceptualization, supervision, and writing (review and editing); and F.L. – conceptualization, formal analysis, visualization (figures), supervision, and writing (original draft, review and editing). Contributions are assigned using CRediT taxonomy (https://casrai.org/credit/).

Conflicts of interest

There are no conflicts to declare.

Acknowledgements

The authors thank the Materials Characterization Facility and Electron Microscopy Facility at the Fondazione Istituto Italiano di Tecnologia for use of XRD and TEM equipment and technical support and Filippo Drago of Nanochemistry Facility for elemental analysis using ICP-OES. Z. H. acknowledges Ghent University (GOA 01G01019) and FWO-Vlaanderen (SBO Proceed) for research funding. E. S., M. C. and F. L. thank Matilde Cirignano for the fruitful suggestions.

Notes and references

1 Q. A. Akkerman, G. Rainò, M. V. Kovalenko and L. Manna, *Nat. Mater.*, 2018, **17**, 1–12.
2 B. Vargas, G. Rodríguez-López and D. Solis-Ibarra, *ACS Energy Lett.*, 2020, **5**, 3591–3608.
3 W. Ke and M. G. Kanatzidis, *Nat. Commun.*, 2019, **10**, 1–4.
4 X. Li, X. Gao, X. Zhang, X. Shen, M. Lu, J. Wu, Z. Shi, V. L. Colvin, J. Hu, X. Bai, W. W. Yu and Y. Zhang, *Adv. Sci.*, 2021, **8**, 1–33.
5 F. Giustino and H. J. Snaith, *ACS Energy Lett.*, 2016, **1**, 1233–1240.
6 J. Luo, X. Wang, S. Li, J. Liu, Y. Guo, G. Niu, L. Yao, Y. Fu, L. Gao, Q. Dong, C. Zhao, M. Leng, F. Ma, W. Liang, L. Wang, S. Jin, J. Han, L. Zhang, J. Etheridge, J. Wang, Y. Yan, E. H. Sargent and J. Tang, *Nature*, 2018, **563**, 541–545.
7 F. Locardi, E. Sartori, J. Buha, J. Zito, M. Prato, V. Pinchetti, M. L. Zaffalon, M. Ferretti, S. Brovelli, I. Infante, L. De Trizio and L. Manna, *ACS Energy Lett.*, 2019, **4**, 1976–1982.
8 N. R. Wolf, B. A. Connor, A. H. Slavney and H. I. Karunadasa, *Angew. Chem., Int. Ed.*, 2021, **60**, 16264–16278.
9 G. Volonakis, A. A. Haghighirad, R. L. Milot, W. H. Sio, M. R. Filip, B. Wenger, M. B. Johnston, L. M. Herz, H. J. Snaith and F. Giustino, *J. Phys. Chem. Lett.*, 2017, **8**, 772–778.
10 S. E. Creutz, E. N. Crites, M. C. De Siena and D. R. Gamelin, *Nano Lett.*, 2018, **18**, 1118–1123.
11 A. Noculak, A. Noculak, V. Morad, V. Morad, K. M. McCall, S. Yakunin, Y. Shynkarenko, S. Yakunin, Y. Shynkarenko, M. Wörle and M. V. Kovalenko, *Chem. Mater.*, 2020, **32**, 5118–5124.
12 F. Locardi, M. Cirignano, D. Baranov, Z. Dang, M. Prato, F. Drago, M. Ferretti, V. Pinchetti, M. Fanciulli, S. Brovelli, L. De Trizio and L. Manna, *J. Am. Chem. Soc.*, 2018, **140**, 12989–12995.
13 Q. Liao, J. Chen, L. Zhou, T. Wei, L. Zhang, D. Chen, F. Huang, Q. Pang and J. Z. Zhang, *J. Phys. Chem. Lett.*, 2020, **11**, 8392–8398.
14 N. K. Nila and N. Angshuman, *Chem. Commun.*, 2018, **54**, 5205–5208.
15 S. Toso, D. Baranov and L. Manna, *ACS Energy Lett.*, 2020, **5**, 3409–3414.
16 B. Vargas, E. Ramos, E. Pérez-Gutiérrez, J. C. Alonso and D. Solis-Ibarra, *J. Am. Chem. Soc.*, 2017, **139**, 9116–9119.
17 T. Cai, W. Shi, S. Hwang, K. Kobbekaduwa, Y. Nagaoka, H. Yang, K. Hills-Kimball, H. Zhu, J. Wang, Z. Wang, Y. Liu, D. Su, J. Gao and O. Chen, *J. Am. Chem. Soc.*, 2020, **142**, 11927–11936.
18 B. Vargas, R. Torres-Cadena, J. Rodríguez-Hernández, M. Gembicky, H. Xie, J. Jiménez-Mier, Y. S. Liu, E. Menéndez-Proupin, K. R. Dunbar, N. Lopez, P. Olalde-Velasco and D. Solis-Ibarra, *Chem. Mater.*, 2018, **30**, 5315–5321.
19 B. Vargas, E. Coutiño-Gonzalez, O. Ovalle-Encinia, C. Sánchez-Aké and D. Solis-Ibarra, *J. Phys. Chem. Lett.*, 2020, **11**, 10362–10367.
20 C. Peng, Q. Wei, L. Chen, R. Zeng, Q. Zhang, Q. Hu and B. Zou, *J. Mater. Chem. C*, 2021, **9**, 15522.
21 N. P. Holzapfel, J. D. Majher, T. A. Strom, C. E. Moore and P. M. Woodward, *Chem. Mater.*, 2020, **32**, 3510–3516.
22 B. Vargas, D. T. Reyes-Castillo, E. Coutino-Gonzalez, C. Sánchez-Aké, C. Ramos, C. Falcony and D. Solis-Ibarra, *Chem. Mater.*, 2020, **32**, 9307–9315.
23 H. Yang, W. Shi, T. Cai, K. Hills-Kimball, Z. Liu, L. Dube and O. Chen, *Nanoscale*, 2020, **12**, 23191–23199.
24 T. Cai, W. Shi, D. J. Gosztol, K. Kobbekaduwa, H. Yang, N. Jin, Y. Nagaoka, L. Dube, J. Schneider, S. Hwang, J. Gao, X. Ma and O. Chen, *Matter*, 2021, **4**, 2936–2295.
25 T. T. Tran, T. T. Tran, C. A. Pocs, Y. Zhang, Y. Zhang, M. J. Winiarski, M. J. Winiarski, J. Sun, M. Lee, T. M. McQueen and T. M. McQueen, *Phys. Rev. B*, 2020, **101**, 235107.
26 B. Pradhan, G. S. Kumar, S. Sain, A. Dalui, U. K. Ghorai, S. K. Pradhan and S. Acharya, *Chem. Mater.*, 2018, **30**, 2135–2142.
27 Y. Jing, Y. Liu, M. Li and Z. Xia, *Adv. Opt. Mater.*, 2021, **9**, 1–15.
28 F. Locardi, M. Samoli, A. Martinelli, O. Erdem, D. V. Magalhaes, S. Bals and Z. Hens, *ACS Nano*, 2021, **15**, 17729–17737.
29 H. Arfin, A. S. Kshirsagar, J. Kaur, B. Mondal, Z. Xia, S. Chakraborty and A. Nag, *Chem. Mater.*, 2020, **32**, 10255–10267.
30 X. Liu, X. Xu, B. Li, L. Yang, Q. Li, H. Jiang and D. Xu, *Small*, 2020, **16**, 1–7.
31 S. He, S. Fang, T. Han, T. Lang, M. Cai, H. You, L. Peng, S. Cao, B. Liu, Q. Qiang, J. Chen and B. Lei, *J. Phys. Chem. C*, 2021, **125**(31), 16938–16945.
32 S. Ji, X. Yuan, S. Cao, W. Ji, H. Zhang, Y. Wang, H. Li, J. Zhao and B. Zou, *J. Phys. Chem. Lett.*, 2020, **11**, 2142–2149.
33 H. Liu, Z. Wu, J. Shao, D. Yao, H. Gao, Y. Liu, W. Yu, H. Zhang and B. Yang, *ACS Nano*, 2017, **11**, 2239–2247.
34 N. Mondal, A. De and A. Samanta, *ACS Energy Lett.*, 2019, **4**, 32–39.
35 M. Imran, J. Ramade, F. Di Stasio, M. De Franco, J. Buha, S. Van Aert, L. Goldoni, S. Lauciello, M. Prato, I. Infante, S. Bals and L. Manna, *Chem. Mater.*, 2020, **32**, 10641–10652.

36 M. Lu, J. Guo, P. Lu, L. Zhang, Y. Zhang, Q. Dai, Y. Hu, V. L. Colvin and W. W. Yu, *J. Phys. Chem. C*, 2019, **123**, 22787–22792.
37 V. G. V. Dutt, S. Akhil and N. Mishra, *ChemNanoMat*, 2020, **6**, 1730–1742.
38 B. A. Koscher, J. K. Swabeck, N. D. Bronstein and A. P. Alivisatos, *J. Am. Chem. Soc.*, 2017, **139**, 6566–6569.
39 J. T. Lin, Y. K. Hu, C. H. Hou, C. C. Liao, W. T. Chuang, C. W. Chiu, M. K. Tsai, J. J. Shyue and P. T. Chou, *Small*, 2020, **16**, 2–9.